ISSN 1063-7761, Journal of Experimental and Theoretical Physics, 2009, Vol. 109, No. 5, pp. 775–785. © Pleiades Publishing, Inc., 2009.
Original Russian Text © S.G. Ovchinnikov, M.M. Korshunov, E.I. Shneyder, 2009, published in Zhurnal Éksperimental'noĭ i Teoreticheskoĭ Fiziki, 2009, Vol. 136, No. 5, pp. 898–909.

ORDER, DISORDER, AND PHASE TRANSITION IN CONDENSED SYSTEM

Lifshits Quantum Phase Transitions and Rearrangement of the Fermi Surface upon a Change in the Hole Concentration in High-Temperature Superconductors

S. G. Ovchinnikov[a,b,e]*, M. M. Korshunov[a,c,d], and E. I. Shneyder[a,e]

[a] *Kirenskii Institute of Physics, Siberian Branch, Russian Academy of Sciences, Krasnoyarsk, 660036 Russia*
[b] *Siberian Federal University, Krasnoyarsk, 660041 Russia*
[c] *Max-Planck-Institut für Physik Komplexer Systeme, D-01187 Dresden, Germany*
[d] *Department of Physics, University of Florida, Gainesville, Florida, 32611 USA*
[e] *Reshetnikov Siberian State Aerospace University, Krasnoyarsk, 660014 Russia*
e-mail: sgo@iph.krasn.ru

Received April 17, 2009

Abstract—Changes in the electronic structure in the normal phase of high-T_c superconductors (HTSCs), viz., layered cuprates, are considered. The results of LDA + GTB calculations of the electron structure and the Fermi surface of $La_{2-x}Sr_xCuO_4$ one-layer cuprates with allowance for strong correlations are compared with ARPES and quantum oscillations data. Two critical points x_{c1} and x_{c2} are discovered at which the rearrangement of the Fermi surface takes place. In the vicinity of these points, changes in the thermodynamic properties at low temperatures are determined using the Lifshits ideology concerning 2.5-order quantum phase transitions. A singularity $\delta(C/T) \propto (x - x_e)^{1/2}$ in the electron heat capacity agrees well with the available experimental data in the vicinity of $x_{c1} \approx 0.15$. Sign reversal of the Hall constant upon doping is also considered qualitatively.

PACS numbers: 64.70.Tg, 71.10.-w, 74.25.Jb

DOI: 10.1134/S1063776109110077

1. INTRODUCTION

HTSC cuprates have been actively studied for more than 20 years and are apparently the best studied class of condensed systems (save for the semiconductor family). The properties of cuprates were found to be peculiar. Not only the origin and mechanisms of superconductivity, but also anomalous properties of the "normal" phase (and primarily the pseudogap state; see reviews [1–8]) are unusual. Vast information on the electronic structure of cuprates was obtained using angle-resolved photoelectron spectroscopy (ARPES) [9], which revealed the rearrangement of the Fermi surface from Fermi arcs at the center of the Brillouin zone at low doping levels into large hole pockets centered at point (π, π) at high doping levels. New results of measurements of quantum oscillations in strong magnetic fields obtained during the last two years for $YBa_2Cu_3O_{6.5}$ [10] and $YBa_2Cu_4O_8$ [11, 12] single crystals, and which indicate the existence of small hole pockets for weakly doped compounds, apparently contradict the Fermi arcs detected by ARPES. This contradiction was removed by taking into account the interaction of holes with short-order antiferromagnetic (AFM) fluctuations, which are strong in the pseudogap state [13–16]. It was found that half a hole pocket is formed by shadow-band states and is blurred due to strong scattering of quasiparticles from these fluctuations. The other half of the hole pocket could be observed only in modern ARPES experiments using a UV laser, which makes it possible to attain high energy resolution [17]. Such strong interactions of charge carriers with magnetic inhomogeneities are typical not only of cuprates, but also other transition-metals oxides with strong electron correlations (e.g., manganites [18]).

Traditional methods of one-electron band theory like local density approximation (LDA) in the density functional method are insufficient for theoretical description of the electronic structure of weakly doped cuprates, the emergence of small hole pockets upon doping of the La_2CuO_4 dielectric, and the dependence of the Fermi surface on concentration. Strong correlations should be taken into account. In the strong electron correlation mode, multiband realistic models of the electronic structure of the CuO_2 layer can be reduced in the low-energy excitation range to the effective Hubbard model and to the t–J model [19–23]. In the LDA + GTB hybrid scheme [24] based on LDA ab initio calculations without fitting parameters and taking into account strong electron correlations in the generalized tight binding (GTB) method [19], the low-energy t–t'–t''–J^* model was obtained from

microscopic analysis; all model parameters were also calculated.

Small hole pockets with an area on the order of x around the $(\pi/2, \pi/2)$ point appear when analyzing the hole dynamics against the background of AFM spin ordering using exact diagonalization methods [25] or the quantum-mechanical Monte Carlo method [26, 27] for finite clusters, as well as for an infinite lattice in various variational methods or in perturbation theory [28–32]. When the long-range AFM order is violated, the calculation of the electronic structure for the paramagnetic state gives another type of dispersion with the top of the valence band at point (π, π) [33]. The Fermi surface in this case is a large hole-type surface with the center at point (π, π). Apologists for "universal metallic dispersion" still exist; they calculate the band structure and the Fermi surface of $La_{2-x}Sr_xCuO_4$ and insist on the applicability of the rigid band model, according to which the Fermi level is shifted under doping relative to an invariable band [34]. After the discovery of small hole pockets in weakly doped cuprates in experiments on quantum oscillations [10–12], scenario [34] becomes completely unconvincing. Instead of the simple paramagnetic state of a normal metal, a pseudogap state is formed in cuprates beyond the AFM ordering region. Although the nature of this state is still disputable, the role of fluctuating short-range AFM order is obvious [5]. It was noted above that it is the inclusion of the interaction of an electron with fluctuating short-range AFM order that has made it possible to match the quantum oscillations and ARPES data for low doping levels. However, a short-range AFM order with a correlation length of $\xi_{AFM} \approx 10$ Å also exists in the optimal doping region [35]; consequently, this should be taken into account not only in analyzing weakly doped systems. At low temperatures $T \leq 10$ K, fluctuations are quite slow, with a characteristic lifetime on the order of 10^{-9} s on scales on the order of ξ_{AFM} (the size of an AFM microdomain) [36]. This time considerably exceeds the characteristic time of restoration of equilibrium for the Fermi system in ARPES measurements ($\sim 10^{-13}$ s) [37] and the period of revolution of an electron in a cyclotron orbit on the Fermi surface ($2\pi\omega_c^{-1} \sim 10^{-12}$ s, where ω_c is the cyclotron frequency in experiments [10, 11]). Thus, calculating the dynamics of a quasiparticle with allowance for short-range AFM order, we can disregard the dynamics of the magnetic order itself and take into account only its spatial inhomogeneity.

In this study, this approach is used to analyze the dependence of the electronic structure and the Fermi surface on concentration. In Section 2, the results of calculating the electronic structure of quasiparticles in the t–t'–t''–J^* model are considered with allowance for the static short-range AFM order, and the change in the Fermi surface topology as a result of doping is demonstrated. The area under the Fermi surface and the Luttinger theorem are also discussed. In Section 3, the results are explained qualitatively. In Section 4, the 2.5-order quantum phase transitions in the charge carrier concentration are considered in accordance with Lifshits' publications [38, 39]; corrections to the electron heat capacity in the vicinity of the transition are compared with the results of measurements [40]. In the Conclusions, the concentration dependence of transport properties is considered qualitatively.

2. THE FERMI SURFACE OF $La_{2-x}Sr_xCuO_4$ AND ITS VARIATIONS WITH THE DOPING LEVEL

We begin the LDA + GTB analysis [24] of the electronic structure using the LDA ab initio calculations underlying the construction of the Wannier function in the basis of p-orbitals for oxygen and e_g-orbitals for copper. In the Wannier representation, we write the multiband p–d-model [41] with ab initio parameters calculated. Then the p–d-model is written in the representation of X operators using cluster perturbation theory [19, 42], and the low-energy effective Hubbard model with effective parameter $U = E_{CT}$, where E_{CT} is the dielectric gap with charge transfer [43], is constructed using the GTB method. In the Hubbard model, operator $X_j^{0\sigma}$ describes the annihilation of a hole at site f in the lower Hubbard band (LHB) of holes, which corresponds to electrons at the bottom of the conduction band. Annihilation of a hole in the upper Hubbard band (UHB) is described by operator $X_f^{\bar{\sigma}2}$, which corresponds to the production of an electron at the top of the valence band. In constructing the t–J model, we can either eliminate two-particle states of holes and obtain the effective Hamiltonian for the LHB, or eliminate two-particle states of electrons (a vacuum of holes, which corresponds to the $d^{10}p^6$-configuration of the CuO_6 cell) and obtain the effective Hamiltonian for the UHB. It is the latter case that is of interest for our study devoted to analysis of the Fermi surface in hole-doped cuprates. All parameters of the t–t'–t''–J^* model obtained in this way for $La_{2-x}Sr_xCuO_4$ were calculated using the LDA + GTB approach (i.e., the Hamiltonian does not contain fitting parameters). Here, J^* indicates that we take into account three-center correlated jumps with an amplitude on the order of J.

The Hamiltonian of this model has the form

$$H_{t-J^*} = H_{t-J} + H_{(3)},$$

$$H_{t-J} = \sum_{f,\sigma}[(\varepsilon - \mu)X_f^{\sigma\sigma} + (\varepsilon_2 - 2\mu)X_f^{22}] + \sum_{f\neq g,\sigma} t_{fg}^{11} X_f^{2\bar{\sigma}} X_g^{\bar{\sigma}2} + \sum_{t\neq g} J_{fg}\left(\mathbf{S}_f \cdot \mathbf{S}_g - \frac{1}{4}n_f n_g\right), \quad (1)$$

$$H_{(3)} = \sum_{f \neq m \neq g,\, \sigma} \frac{t_{fm}^{01} t_{mg}^{01}}{U_{\text{eff}}} (X_f^{\sigma 2} X_m^{\bar{\sigma}\sigma} X_g^{2\bar{\sigma}} - X_f^{\bar{\sigma}2} X_m^{\sigma\sigma} X_g^{2\bar{\sigma}}).$$

Here, $J_{fg} = 2(t_{fg}^{01})^2/U_{\text{eff}}$, t_{fg}^{01} is the parameter of hopping between the fth and the gth atoms with the LHB $\longleftrightarrow$ UHB transitions between the bands, $\mathbf{S}_f$ is the spin operator, ε and ε_2 are the local energies of one and two holes, and μ is the chemical potential. Intraband hopping parameters t_{fg}^{11} were calculated up to the sixth coordination sphere; it was found that the contribution of the fourth and subsequent neighbors to the dispersion relation is negligibly small. The introduction of three hopping parameters t, t', and t'' is usually substantiated as the necessity of fitting dispersion to ARPES. It can be seen, however, that there also exists a microscopic substantiation of the introduction of parameters t, t', and t''. The model parameters (in electronvolts) obtained for $La_{2-x}Sr_xCuO_4$ are as follows:

$$\begin{aligned} t &= 0.932, \quad t' = -0.12, \quad t'' = 0.152, \\ J &= 0.298, \quad J' = 0.003, \quad J'' = 0.007. \end{aligned} \tag{2}$$

For the Green's function of a hole in the UHB ($\bar{\sigma} \equiv -\sigma$),

$$G_\sigma(\mathbf{k}, E) = \langle\langle X_{\mathbf{k}}^{\bar{\sigma}2} | X_{\mathbf{k}}^{2\bar{\sigma}} \rangle\rangle_E, \tag{3}$$

we can write the following exact representation (generalized Dyson equation) obtained from analysis of the complete series of diagrams in perturbation theory for the X-operators [44]:

$$G_\sigma(\mathbf{k}, E) = \frac{P_\sigma(\mathbf{k}, E)}{E - \varepsilon_0 + \mu - P_\sigma(\mathbf{k}, E) t_{\mathbf{k}} - \sum_\sigma(\mathbf{k}, E)}, \tag{4}$$

where $t_{\mathbf{k}}$ is the Fourier transform of the hopping parameter and $P_\sigma(\mathbf{k}, E)$ and $\sum_\sigma(\mathbf{k}, E)$ are the force and mass operators. The simplest Hubbard-I mean field approximation corresponds to $\sum_\sigma = 0$, $P_\sigma = F_{\bar{\sigma}2} = \langle X_f^{\bar{\sigma}\bar{\sigma}} \rangle + \langle X_f^{22} \rangle$. In this case, the spectral weight of a quasiparticle is defined by filling factor $F_{\bar{\sigma}2}$ as the sum of the occupation numbers of the initial and final states $|2\rangle$ and $|\bar{\sigma}\rangle$. In the diagrammatic technique [45], this factor is referred to as the end factor.

To take into account the short-range magnetic order, we must go beyond the Hubbard-I approximation. The computational method is described in detail in [46], where it was used for analyzing the dispersion relation in the LHB. The method is based on projecting higher-order Green's functions onto function (3) and is a modification of the Mori projection technique. A similar method taking into account the dynamics of spin correlations was used in [23, 47]. Considering that the total number of holes per $La_{2-x}Sr_xCuO_4$ molecule is $n_h = 1 + x$ and that the condition of completeness of the basis for the Hilbert space in the t–J model is

$$\sum_\sigma X_f^{\sigma\sigma} + X_f^{22} = 1, \tag{5}$$

we can easily find occupation numbers $\langle X_f^{\sigma\sigma} \rangle = (1 - x)/2$ and $\langle X_f^{22} \rangle = x$. In this case, the filling factor is $F_{\sigma 2} = (1 + x)/2$. As a result, Green's function (3) assumes the form

$$G_\sigma(\mathbf{k}, E) = \frac{(1+x)/2}{E - \varepsilon_0 + \mu - \frac{1+x}{2} t_{\mathbf{k}} - \frac{1-x^2}{4} (t_{\mathbf{k}}^{01})^2 / U_{\text{eff}} - \sum(\mathbf{k})}, \tag{6}$$

where the mass operator is

$$\begin{aligned} \sum(\mathbf{k}) = \frac{2}{1+x} \frac{1}{N} \sum_{\mathbf{q}} \Bigg\{ \Bigg[t_{\mathbf{q}} - \frac{1-x}{2} J_{\mathbf{k}-\mathbf{q}} \\ - x \frac{(t_{\mathbf{q}}^{01})^2}{U_{\text{eff}}} - (1+x) \frac{t_{\mathbf{k}}^{01} t_{\mathbf{q}}^{01}}{U_{\text{eff}}} \Bigg] K(\mathbf{q}) + \Bigg[t_{\mathbf{k}-\mathbf{q}} - \frac{1-x}{2} \\ \times \left(J_{\mathbf{q}} - \frac{(t_{\mathbf{k}-\mathbf{q}}^{01})^2}{U_{\text{eff}}} \right) - \frac{(1+x) t_{\mathbf{k}}^{01} t_{\mathbf{k}-\mathbf{q}}^{01}}{U_{\text{eff}}} \Bigg] \frac{3}{2} C(\mathbf{q}) \Bigg\}. \end{aligned} \tag{7}$$

Here, $K(\mathbf{q})$ and $C(\mathbf{q})$ denote the kinematic and spin correlation functions,

$$\begin{aligned} K(\mathbf{q}) &= \sum_{\mathbf{f}-\mathbf{g}} e^{-i(\mathbf{f}-\mathbf{g})\cdot\mathbf{q}} \langle X_{\mathbf{f}}^{2\bar{\sigma}} X_{\mathbf{g}}^{\bar{\sigma}2} \rangle, \\ C(\mathbf{q}) &= \sum_{\mathbf{f}-\mathbf{g}} e^{-i(\mathbf{f}-\mathbf{g})\cdot\mathbf{q}} \langle X_{\mathbf{f}}^{\alpha\bar{\sigma}} X_{\mathbf{g}}^{\bar{\sigma}\sigma} \rangle \\ &= 2 \sum_{\mathbf{f}-\mathbf{g}} e^{-i(\mathbf{f}-\mathbf{g})\cdot\mathbf{q}} \langle S_{\mathbf{f}}^z S_{\mathbf{g}}^z \rangle. \end{aligned} \tag{8}$$

An analogous Green's function for the lower Hubbard subband, which is filled in our case upon electron doping, was obtained earlier in [48]. We assume that the spin liquid is isotropic and the correlation functions are the same for all three spin components. The kinematic correlators can be expressed directly in terms of electron Green's function (3), while the spin correlator for the t–J^*-model (taking into account the three-center terms) was calculated analogously to [48] using the method developed for the Heisenberg model in [49, 50]. The resultant static magnetic susceptibility for the t–J-model is in good agreement with the results of calculations based on other methods [51, 52].

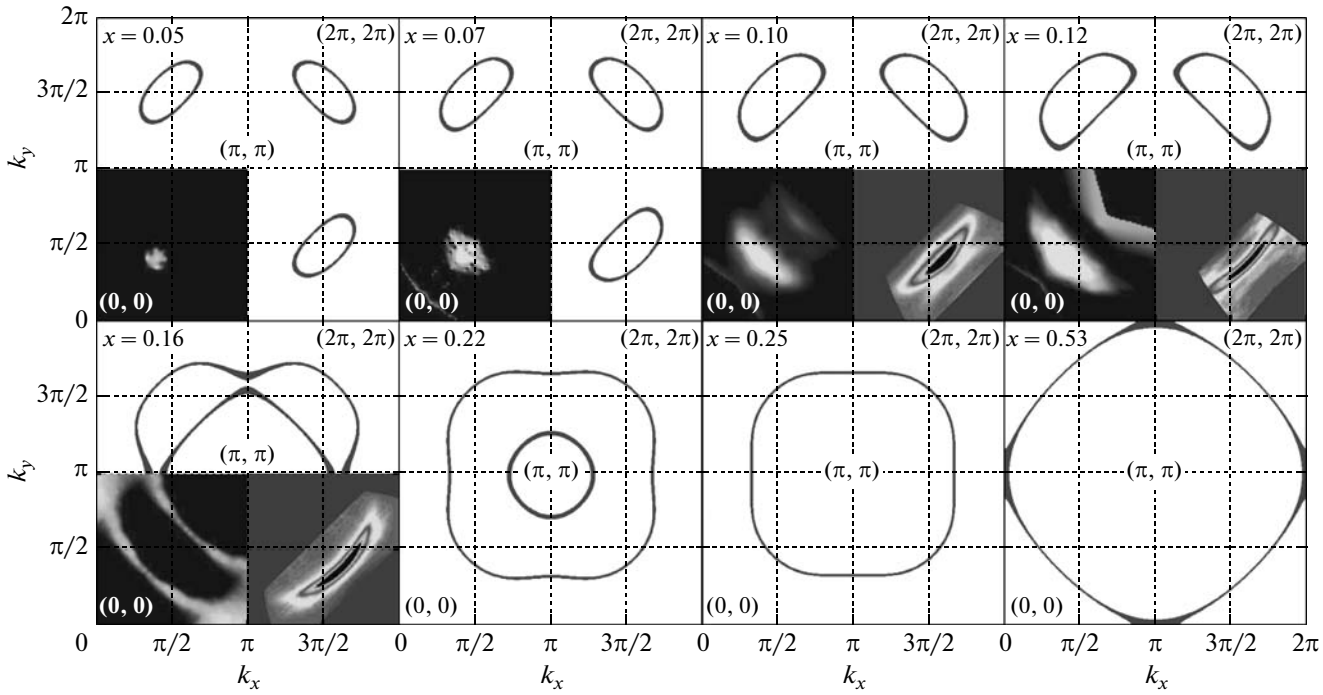

Fig. 1. Cross sections of the Fermi surface in $La_{2-x}Sr_xCuO_4$ for various doping levels. Modifications of topology take place at $x_{c1} \approx 0.15$ and $x_{c2} \approx 0.24$. Experimental ARPES data [57] are given in the lower left corner; the results obtained in [17] for $x = 0.12$ are shown in the lower right corner.

Self-consistent calculation of correlators (8) and chemical potential μ with parameters (2) has made it possible to construct a family of Fermi surfaces for various doping levels (Fig. 1). For a low doping level, four hole pockets exist near points $(\pi/2, \pi/2)$ as expected for a hole in the AFM phase. In the vicinity of point $x_{c1} \approx 0.15$, a constriction is formed on the $(\pi, 0)$–(π, π) line and the Fermi surface topology changes. For $x_{c1} < x < x_{c2} \approx 0.24$, we have two surfaces centered at point (π, π). The smaller pocket is of the electron type (see Fig. 3 below) and vanishes for $x \longrightarrow x_{c2}$. The large hole pocket becomes more and more rounded with increasing x, and only this pocket is preserved for $x > x_{c2}$. Finally, for $x = x_{c3}$, the hole-type surface is transformed into an electron-type surface with the center at point Γ.

It should be noted that the values of critical concentrations were calculated to a finite degree of accuracy. First, parameters of the t–t'–t''–J^* model were obtained as a result of a complex procedure of LDA projection of wavefunctions in the basis of Wannier functions and may slightly change if the basis of the latter functions is modified. Second, the method for determining Green's functions (6) is approximate; the inclusion of higher-order contributions may change the quantitative values of critical points. It will be shown in the next section that the qualitative pattern will hardly change since it is determined by the general properties of electron dispersion against the background of fluctuating short-range AFM order. It should also be noted that such modifications of the Fermi surface were obtained for the Hubbard model using a more refined approach, in which not only the real, but also the imaginary part of the mass operator is taken into account (see Fig. 15 in [47]), as well as in calculations based on the spin-fermion model [53] and Hubbard model taking into account spin density wave fluctuations. An analogous transformation with the emergence of a doubly connected Fermi surface in the range of intermediate compositions was obtained recently in the quantum-chemical ab initio calculations with allowance for multielectron $(N-1)$, N, and $(N+1)$ configurations [56]. Qualitative agreement between our results and the results of calculations [47, 53, 56] carried out using different approximations is due to the fact that these results are based on same main idea: the electronic structure is determines by short-range magnetic order in all cases. However, the evolution of the electronic structure is self-consistently connected with the magnetic order evolution only in our study.

In Fig. 1, our calculations of the Fermi surface are compared to the ARPES data [57] obtained on $Bi_2Sr_{2-x}La_xCuO_{6+y}$ (Bi2201) single crystals for various hole concentrations p per CuO_2 cell, $0.05 < p < 0.18$. This crystal, like $La_{2-x}Sr_xCuO_4$, has a single CuO_2 plane in the unit cell; consequently, our calculations for one-layer cuprates are completely applicable provided that $p = x$. As regards the model parameters, we must assume, following [57], that these parameters

in the one-electron approach strongly depend on concentration even for the same substance with different doping levels. The authors of [57] speak of the difference in the values of t'/t for Bi2201 and $La_{2-x}Sr_xCuO_4$ precisely in connection with the dependence on the doping level (it can be seen from Figs. 5a and 5b in [57] that the values of t'/t for the two substances almost coincide for the lowest doping level). In our multielectron approach, the same parameters were calculated ab initio in the underdoped case and are assumed to be independent of the doping level. For this reason, our values of hopping parameters should not necessarily coincide with the results of fitting in the one-electron method. Since the lattice parameters of the copper–oxygen layer for Bi2201 and $La_{2-x}Sr_xCuO_4$ differ insignificantly, we believe that qualitative comparison of our results with experiment [57] is justified. It can be seen that for concentrations of $x = 0.05$, 0.07, 0.10, and 0.12, part of the hole pocket (arc) closest to point Γ is visible. Another part, which is closer to point (π, π), has a small barely visible spectral weight. However, this part can be seen in the ARPES spectra even for $x = 0.10$ and 0.12. In the lower right corner of the figure, the results of recent ARPES measurements with ultrahigh resolution [17] are shown for $x = 0.12$; weak signals shifted relative to $(\pi/2, \pi/2)$ and having an intensity an order of magnitude lower than the intensity in the arc were observed. Thus, the "arc–pocket" contradiction has been removed experimentally. For $x = 0.11$, a small pocket was also observed in [17], but it is not seen for $x = 0.10$ and 0.16. The absence of a pocket for $x = 0.10$ cannot be substantiated, but the situation for $x = 0.16$ is different. For $x = 0.16$ (i.e., after passage through the critical point), our calculations are in good agreement with two cross sections of the Fermi surface. And although the Fermi surface closest to point (π, π) in Bi-cuprate single crystals is traditionally attributed to superstructural reflections, such an exact coincidence of our calculation with experiments is hardly accidental. It cannot be ruled out that the very fact of the formation of the superstructure is associated with rearrangement of the Fermi surface. Another possible scenario is associated with the fact that the ARPES signal from the superstructure masks one of the theoretically obtained cross sections of the Fermi surface. Finally, the third and most plausible explanation is associated with the effect of scattering from AFM fluctuations, which suppresses the spectral intensities of the peaks corresponding to the Fermi surface closest to the (π, π) point. This scenario will be discussed in detail in the next section.

In the case of strong doping (e.g., for $Tl_2Ba_2CuO_{6+y}$ with $p \approx 0.26$), ARPES shows a large hole pocket with the center at point (π, π) [58]. An analogous Fermi surface was observed in ARPES measurements for $La_{2-x}Sr_xCuO_4$ with $x = 0.22$. Our calculations for $x > x_{c2}$ show precisely this Fermi surface.

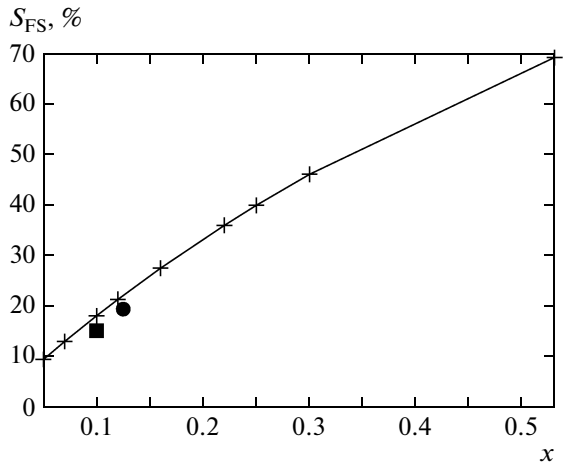

Fig. 2. Dependence of the area of the hole-type Fermi surface (in percent of the area of the Brillouin zone) on the doping level (crosses). The solid curve corresponds to the predictions of the generalized Luttinger theorem [60] in accordance with the $2x/(1 + x)$ dependence. The experimentally determined values of areas from [10, 11] are shown by symbols (■ for $YBa_2Cu_3O_{6.5}$ ($p = 0.1$) and ● for $YBa_2Cu_4O_8$ ($p = 0.125$).

According to the results obtained in [59], an electron pocket is observed for $La_{2-x}Sr_xCuO_4$ even for $x = 0.30$.

Let us consider the concentration dependence of the area under the Fermi surface and the situation with the Luttinger theorem. Figure 2 shows the dimensionless area of the Fermi surface as a percentage of the area of the Brillouin zone. It should be noted that in the conventional formulation, the Luttinger theorem for Hubbard fermions does not hold because of the redistribution of the spectral weight of a free electron among various Hubbard fermions. Indeed, for free electrons, each filled cell of the k-space contains two electrons. For Hubbard fermions, for which the spectral weight is defined in the general form by the force operator (numerator of Green's function (4))—while in our approach it is determined by filling factor $F_{\bar{\sigma}2} = (1 + x)/2$—each filled cell contains (with allowance for spin) not two but $2F_{\bar{\sigma}2} = 1 + x$ electrons. As a result, the generalized Luttinger theorem was proposed for Hubbard fermions [60], in which each filled state is taken into account with its own spectral weight.

In our case, for $La_{2-x}Sr_xCuO_4$, the hole concentration is $n_h = 1 + x$, while the electron concentration is $n_e = 1 - x$. In accordance with dispersion relations for electrons, the number N_k^e of states occupied by electrons (k) below the Fermi level was calculated for each doping level (see Fig. 3b below). Taking into account the spectral weight and carrying out summation over spin, we find that the electron concentration is $n_e = 2F_{\bar{\sigma}2}N_k^e = 1 - x$. This gives $N_k^e = (1 - x)/(1 + x)$.

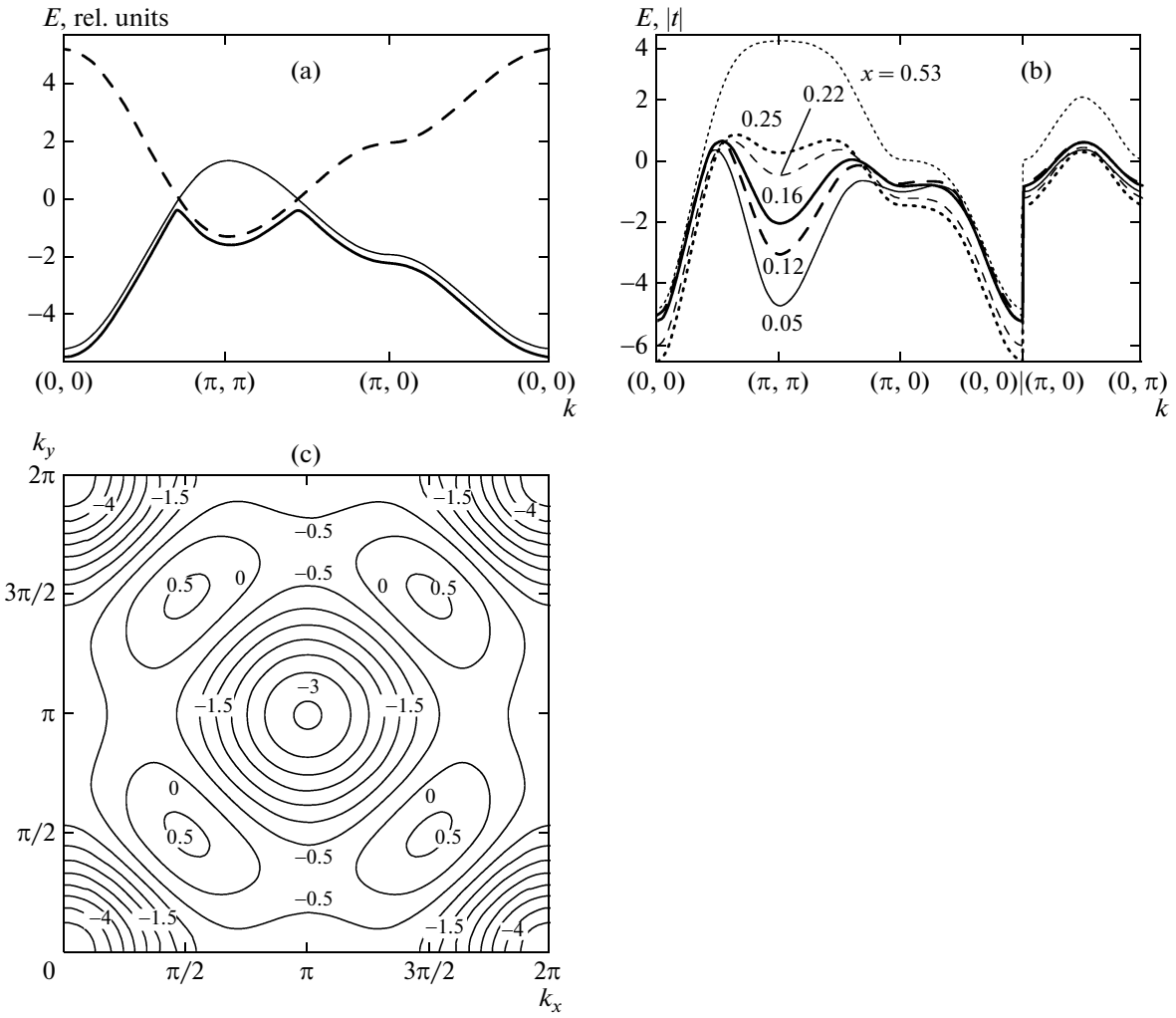

Fig. 3. (a) Qualitative scheme of formation of the band structure of electrons in the spin-liquid state from the electronic structure in the paramagnetic phase; (b) results of our calculation of the dispersion relation from Green's function (6) for various values of concentration (Fermi level is determined from the condition $\varepsilon = 0$); and (c) constant-energy sections for a doling level of 0.10, indicating the change in the topology upon a decrease in energy of the same type as on the Fermi surface upon doping. The numbers on isolines correspond to dimensionless energy in the units of the hopping parameter e/t.

The number of states (k) occupied by holes is $N_k^h = 1 - N_k^e = 2x/(1 + x)$. This dependence is shown in Fig. 2 by the solid curve; symbols indicate the numbers N_k^e of occupied electron states calculated using the dispersion relation. The areas obtained in experiments on quantum oscillations are also shown in Fig. 2. It is very important that the Luttinger theorem in its conventional formulation is obviously violated, indicating the inapplicability of the standard pattern of a Fermi liquid. However, we have demonstrated that the generalization of the Luttinger theorem to the case of strongly correlated Hubbard fermions correctly describes the experimentally observed pattern. It should also be noted that experimental data [10–12] prevent us from determining the positions of small pockets in the Brillouin zone; consequently, it is the closeness of the measured and calculated areas of the Fermi surface that demonstrates qualitative agreement with experiment and may indicate the position of pockets.

3. THE QUALITATIVE PATTERN OF ELECTRON DISPERSION AND ARPES IN A SYSTEM WITH FLUCTUATING SHORT-RANGE AFM ORDER

In this section, we use the results obtained in [13–16], which show how AFM fluctuations transform a hole pocket into a finite arc for a low doping level, and we extend these ideas to the entire doping range in which AFM fluctuations are strong. The resultant pat-

tern reproduces the changes in the Fermi surface described above at the quantitative level.

It was shown in [16] that for electrons in a square lattice, which are scattered in a static random field imitating short-range AFM order with wavevector $Q = (\pi, \pi)$, the Green's function can be written in the form

$$G_D(\mathbf{k}, E) = \frac{E - \varepsilon(\mathbf{k}+\mathbf{Q}) + iv k}{(E-\varepsilon(\mathbf{k}))(E-\varepsilon(\mathbf{k}+\mathbf{Q})+iv k) - |D|^2}. \quad (9)$$

Here, $|D|$ indicates the amplitude of fluctuating AFM order and $\varepsilon(\mathbf{k})$ is the electron dispersion in the paramagnetic state,

$$v = |v_x(\mathbf{k}+\mathbf{Q})| + |v_y(\mathbf{k}+\mathbf{Q})|, \quad v_{x,y}(\mathbf{k}) = \partial\varepsilon(\mathbf{k})/\partial k_{x,y}. \quad (10)$$

In the absence of damping, function (9) describes an electron in the state of a spin density wave with the long-range AFM order. However, in the spin-liquid concentration range, long-range order does not exist, and instead of umklapp process $\varepsilon(\mathbf{k}) \longrightarrow \varepsilon(\mathbf{k}+\mathbf{Q})$, we have a dynamic decay with a finite lifetime of $1/\tau \sim v\mathbf{k}$.

The thin curve in Fig. 3a shows typical dispersion $\varepsilon(\mathbf{k})$ emerging in LDA calculations as well as in the t–J-model in the paramagnetic state. The dashed curve shows the spectrum of the shadow zone $\varepsilon(\mathbf{k}+\mathbf{Q})$ reflected specularly from the Fermi level. As a result of repulsion of two branches, a dispersion relation that takes into account the short-range order (bold curve) is formed. The peaks of the spectral function with maxima corresponding to the dashed curve have a finite width due to the finite lifetime. Figure 3b shows the dispersion for various concentrations, which is determined from Green's function (6) and used above for calculating the Fermi surface. The family of constant-energy cross sections for the band structure depicted in Fig. 3b for $x = 0.10$ is shown in Fig. 3c for $x = 0.10$. A value of the chemical potential slightly smaller than zero corresponds to $x < x_{c1}$ in Fig. 3 and leads to small hole pockets near $(\pi/2, \pi/2)$. As the chemical potential decreases, a new intersection with the curve corresponding to the dispersion relation along the $(\pi, 0)$–(π, π) line corresponds to $x = x_{c1}$. Decreasing further, the value of chemical potential approaches the minimum at point (π, π) of the band (hence, it can be concluded that the small pocket near (π, π) is of electron origin). At point x_{c2}, the electron pocket disappears. A further decrease in the chemical potential corresponds to $x > x_{c2}$ and leads to the formation of a large hole pocket with the center at (π, π). In this qualitative analysis, we have used the rigid band model. Actual calculations given in Fig. 3b show a strong dependence of dispersion on the doping level, which means that the rigid band model does not hold quantitatively. Nevertheless, it can be seen that the qualitative pattern in Fig. 3a satisfactorily reproduces the result of our calculation.

Using this qualitative pattern, we can explain the effect of quasiparticle damping on the observed ARPES data. First, in accordance with the conclusions drawn in [13–16, 47], it can be seen that for $x < x_{c1}$, there are two intersections with the hole pocket in the $(0, 0)$–(π, π) direction. The intersection closer to point Γ is mainly formed by the $\varepsilon(\mathbf{k})$ zone without damping, while the intersection closer to (π, π) is due to the contribution of damped states of the shadow zone $\varepsilon(\mathbf{k}+\mathbf{Q})$. For these states, damping blurs the central peak, and these states are not seen in ARPES; only the arcs are visible. A decrease in the spectral weight of quasiparticles without their damping for a region of the shadow zone in the hole pocket, which also explains the formation of the arc, was obtained for spin polarons in [53].

Second, we can extend this analysis to the range of $x > x_{c1}$. It can be seen that the larger pocket is formed by undamped electrons, while the small inner pocket is formed by damped electrons. This is apparently why it is not seen in ARPES. At the same time, as x approaches x_{c2}, Fermi momentum $\mathbf{k_F}$ tends to (π, π). In accordance with relations (10), velocity $v = 0$ at this point. Thus, the small electron pocket for $x \longrightarrow x_{c2}$ is formed by weakly damped quasiparticles. For $x > x_{c2}$, the large hole pocket is formed by undamped quasiparticles and can be clearly seen in ARPES.

Further transformation of the hole Fermi surface into the electron Fermi surface at $x = x_{c3}$ (according to the data from [59], the electron Fermi surface is formed for $La_{2-x}Sr_xCuO_4$ even for $x = 0.30$) occurs in the strong doping region, in which the magnetic correlation length is comparable to the lattice parameters. In this case, analysis based on Green's function (9) is no longer applicable. Although our calculations based on function (6) show the change in the Fermi surface type from the hole- to electron-type surface at point x_{c3}, the value of $x_{c3} = 0.53$ itself is not large as compared to the experimental value. This is not surprising since perturbation theory in the X operator representation is applicable to a doped Mott dielectric with small values of x.

4. PECULIARITIES OF LOW-TEMPERATURE THERMODYNAMICS IN THE VICINITY OF LIFSHITS TRANSITIONS

It was shown in previous sections that a constriction appears on the Fermi surface at point x_{c1} upon an increase in the doping level, and the electron pocket at point x_{c2} disappears. These two singularities in the Fermi surface topology lead to the 2.5-order electron phase transitions according to Lifshits [38, 39] or, in contemporary terminology, to quantum phase transitions. The emergence of a new pocket on the Fermi surface at $\varepsilon = \varepsilon_c$ leads to the addition of $\delta g(\varepsilon) = \alpha(\varepsilon - \varepsilon_c)^{1/2}$ to the density of states. It should be noted that the dispersion relation for cuprates is three-dimensional in spite of clearly manifested anisotropy. Weak jumps

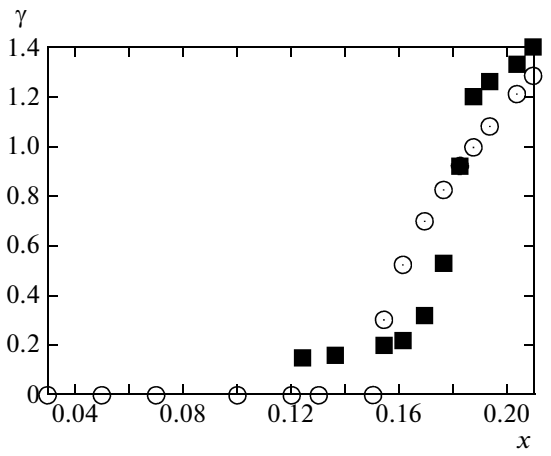

Fig. 4. Variation of the Sommerfeld parameter in the vicinity of the Lifshits transition (○) and experimental data for $\gamma = C_e/T$ at $T = 10$ K (■) borrowed from [40].

between the layers lead to corrugation of the Fermi surface along vector k_z, which was observed in ARPES. For example, various cross sections of the Fermi surface are considered in [33] using LDA calculations and ARPES data. Consequently, we can use the results obtained by Lifshits [38, 39] with minimal modifications. These modifications are due to a decrease in the spectral weight of Hubbard fermions, which is described by filling factor $F = (1 + x)/2$ and appears in the numerator of Green's function (6).

In the vicinity of the critical point, the thermodynamic potential has the form

$$\Omega(\mu, T) = \Omega_0(\mu, T) + \delta\Omega. \tag{11}$$

The correction appearing due to the formation of a new pocket for $\varepsilon > \varepsilon_c$ can be written in the form

$$\delta\Omega = -\int_0^\infty \delta N(\varepsilon) f_F(\varepsilon) d\varepsilon, \tag{12}$$

where $f_F(\varepsilon)$ is the Fermi distribution function, and the number of states with allowance for spectral weight is ($\alpha \sim 1$)

$$\delta N(\varepsilon) = \begin{cases} 0, & \varepsilon < \varepsilon_c \\ \frac{2}{3}\alpha\frac{1+x}{2}(\varepsilon - \varepsilon_c)^{3/2}, & \varepsilon > \varepsilon_c. \end{cases} \tag{13}$$

As a result, at $T \ll z$, where $z = \mu - \varepsilon_c$, in the vicinity of $z = 0$, we obtain

$$\delta\Omega = \begin{cases} -\frac{\sqrt{\pi}}{4}(1+x)\alpha T^{5/2} e^{-|z|/T}, & z < 0 \\ -\frac{2}{15}(1+x)\alpha|z|^{5/2} - \frac{\pi^2}{12}(1+x)T^2|z|^{1/2}, & z > 0. \end{cases} \tag{14}$$

The $z^{5/2}$ singularity indicates a 2.5-order transition in accordance with the Ehrenfest classification. In our case, z varies depending on the doping level, $z(x) = 0$ for $x = x_{c1}$ and $x = x_{c2}$.

We can easily show that the jump in Sommerfeld parameter $\gamma = C_e/T$, where C_e is the electron heat capacity, in the vicinity of the Lifshits transition is given by

$$\delta\gamma = -\frac{\partial^2 \delta F}{\delta T^2}$$

$$= \begin{cases} \frac{\sqrt{\pi}}{4}(1+x)\alpha\frac{|z|^2}{T^2}\left(1 + 3\frac{T}{|z|} + \frac{15}{4}\frac{T^2}{|z|^2}\right) \\ \times e^{-|z|/T}, \quad z < 0 \\ \frac{\pi^2}{6}(1+x)\alpha z^{1/2}, \quad z > 0. \end{cases} \tag{15}$$

The above calculations of the electronic structure resulted in dependence $z(x)$ in the vicinity of each critical point. This dependence is close to linear. Figure 4 illustrates the behavior of the electron heat capacity near $x = x_{c1}$, calculated for $T = 10$ K. The experimental points are plotted from the temperature dependences of $\gamma = C_e/T$ for various values of x in $La_{2-x}Sr_xCuO_4$ [40]. The heat capacity and the electron contribution to entropy in the normal phase were obtained by extrapolation of the results of measurements above superconducting transition temperature T_c to the range of low temperatures. The experimental points in Fig. 4 correspond to total parameter γ, which is given by the following expression in the vicinity of the transition:

$$\gamma(x) = \gamma_0(x) + \delta\gamma; \tag{16}$$

here, γ_0 is a function of x, which is smooth in the vicinity of transition, and $\delta\gamma$ has root singularity (15). The dependence of the spectral weight on the doping level also makes a contribution to the concentration dependence of the heat capacity singularity.

In the vicinity of the second Lifshits transition ($x = x_{c2}$), analogous dependences of thermodynamic parameters are observed. Since the electron pocket disappears upon an increase in x, we have $z > 0$ for $x < x_{c2}$. Since we are not aware of detailed experimental data in the vicinity of x_{c2} with a large number of points for x, and since the dependence of singularity $\delta\gamma$ is defined by the same formula (15), we do not plot its dependence in the vicinity of x_{c2}. In a later publication [61] devoted to measurement of the electron heat capacity of $NdBa_2Cu_3O_{6+y}$, Fig. 9 gives the concentration dependence $\gamma(x)$ with weak singularities near $p = 0.16$ and 0.23, corresponding to our critical points x_{c1} and x_{c2}. However, measurements in [61] were taken at $T = 200$ K and all singularities are blurred.

A series of rearrangements of the Fermi surface upon doping was observed still earlier [29] using the variational solution in the t–J-model. In [29], a small hole pocket was obtained in the AFM phase in the vicinity of point $(\pi/2, \pi/2)$. An electron pocket with the center at point (0, 0) was also obtained for a very large value of x. However, the Fermi surface for intermediate values of x is not in conformity with either our surface or the experimentally observed one. The Lifshits quantum transition in cuprates was discussed earlier mainly in connection with a change in the type of the Fermi surface from the hole to the electron type, which takes place in one-electron calculations when the Fermi level intersects the saddle point $(0, \pi)$ [62]). In our case, this transition occurs at point x_{c3}. Transitions resulting in the formation of an electron pocket at point x_{c1} and its collapse at point x_{c2} have not been discussed to our knowledge.

5. CONCLUSIONS

The sign reversal in charge carriers under doping has been discussed by many authors in recent years. For a large value of x, the hole-type Fermi surface is transformed into an electron-type surface; this was deduced theoretically by many authors and observed experimentally in $La_{2-x}Sr_xCuO_4$ films with $x > 0.30$ [63]. The sign reversal of Hall constant R_H reported for weakly doped cuprates is more surprising. For example, in strong magnetic fields of 50–60 T suppressing superconductivity, sign reversal of R_H was observed for $YBa_2Cu_3O_y$ with $p = 0.10$, 0.12, and 0.14 [64], as well as in $La_{2-x}Sr_xCuO_4$ with $p = 0.11$ [65]. All these samples belong to concentration range $x < x_{c1}$, in which only a hole pocket exists according to our calculations. Probably, the results obtained in [66] may provide a qualitative explanation of this effect. According to [66], convex and concave parts of the Fermi surface for 2D metals with an arbitrary Fermi surface geometry are characterized by opposite signs of the Hall constant. In our case, for $x < x_{c1}$, one side of the hole pocket is convex and the other side is concave (see Fig. 1).

As regards the second Lifshits transition at $x = x_{c2}$, the measurements of low-temperature transport properties of $La_{1.6-x}Nd_{0.4}Sr_xCuO_4$ in strong magnetic fields up to 35 T suppressing superconductivity revealed a modification of the Fermi surface at critical point $p^* \approx 0.23$ [67], which is very close to our point x_{c2}. In accordance with our results, measurements of R_H at $p = 0.24$ indicate a large cylindrical surface containing $1 + p$ holes. At $p = 0.20$ (i.e., below x_{c2}), an increase in the value of $R_H(T)$ at low temperatures indicates a modification of the Fermi surface. It should be noted that critical point x_{c2} itself for the Bi2201 system can be juxtaposed to concentration $p_c = 0.23$, at which the Fermi level in ARPES measurements coincides with the Van Hove singularity [68, 69].

The existence of a quantum critical point to which pseudogap temperature $T^*(x)$ tends when $T \longrightarrow 0$ has been widely discussed in the literature, where the values of $P_{crit} = 0.19$ [70] and 0.27 [71] can be encountered. These data are based on extrapolation and their accuracy is not high. In addition, the pseudogap is hardly the property of the ground state [8]. The critical points obtained in this study are characteristics of the ground state and are connected with the 2.5-order Lifshits phase transitions.

ACKNOWLEDGMENTS

The authors thank A.A. Kordyuk for discussion of the results and T.M. Ovchinnikova for technical assistance in data processing.

This study was supported by the program "Quantum Physics of Condensed Media" of the Presidium of the Russian Academy of Sciences (project no. 5.7), integrated project no. 40 of the Siberian Branch–Ural Division of the Russian academy of Sciences, and the Russian Foundation for Basic Research (project no. 09-02-00127).

REFERENCES

1. E. Dagotto, Rev. Mod. Phys. **66**, 763 (1994).
2. E. G. Maksimov, Usp. Fiz. Nauk **170** (10), 1033 (2000) [Phys.—Usp. **43** (10), 965 (2000)].
3. M. Imada, A. Fujimori, and Y. Tokura, Rev. Mod. Phys. **70**, 1039 (1998).
4. S. G. Ovchinnikov, Usp. Fiz. Nauk **167** (10), 1043 (1997) [Phys.—Usp. **40** (10), 993 (1997)].
5. M. V. Sadovskiĭ, Usp. Fiz. Nauk **171** (5), 540 (2001) [Phys.—Usp. **44** (5), 515 (2001)].
6. V. F. Elesin, V. V. Kapaev, and Yu. V. Kopaev, Usp. Fiz. Nauk **174** (9), 1017 (2004) [Phys.—Usp. **47** (9), 949 (2004)].
7. Yu. A. Izyumov and E. Z. Kurmaev, Usp. Fiz. Nauk **178** (1), 25 (2008) [Phys.—Usp. **51** (1), 23 (2008)].
8. P. A. Lee, Rep. Prog. Phys. **71**, 012 501 (2008).
9. A. Damascelli, Z. Hussein, and Z. X. Shen, Rev. Mod. Phys. **75**, 473 (2003).
10. N. Doiron-Leyraud, C. Proust, D. LeBoeuf, J. Levallois, J.-B. Bonnemaison, R. Liang, D. A. Bonn, W. N. Hardy, and L. Taillefer, Nature (London) **447**, 565 (2007).
11. E. A. Yelland, J. Singleton, C. H. Mielke, N. Narrison, F. F. Balakirev, B. Dabrowski, and J. R. Cooper, Phys. Rev. Lett. **100**, 047 003 (2008).
12. A. F. Bangura, J. D. Fletcher, A. Carrington, et al., Phys. Rev. Lett. **100**, 047004 (2008).
13. E. Z. Kuchinskii, I. A. Nekrasov, and M. V. Sadovskii, Pis'ma Zh. Éksp. Teor. Fiz. **82** (4), 217 (2005) [JETP Lett. **82** (4), 198 (2005)].
14. E. Z. Kuchinskii and M. V. Sadovskii, Zh. Éksp. Teor. Fiz. **130** (3), 447 (2006) [JETP **103** (3), 415 (2006)].
15. N. Harrison, R. D. McDonald, and J. Singleton, Phys. Rev. Lett. **99**, 206 406 (2007).

16. E. Z. Kuchinskii and M. V. Sadovskii, Pis'ma Zh. Éksp. Teor. Fiz. **88** (3), 224 (2008) [JETP Lett. **88** (3), 192 (2008)].
17. J. Meng, G. Liu, W. Zhang, L. Zhao, H. Liu, X. Jia, D. Mu, S. Liu, X. Dong, W. Lu, G. Wang, Y. Zhou, Y. Zhu, X. Wang, Z. Xu, C. Chen, and X. J. Zhou, arXiv:0906.2682.
18. M. Yu. Kagan and K. I. Kugel', Usp. Fiz. Nauk **171** (6), 577 (2001) [Phys.—Usp. **44** (6), 553 (2001)].
19. S. G. Ovchinnikov and I. S. Sandalov, Physica C (Amsterdam) **161**, 607 (1989).
20. S. V. Lovtsov and V. Yu. Yushankhai, Physica C (Amsterdam) **179**, 159 (1991).
21. J. H. Jefferson, H. Eskes, and L. F. Feiner, Phys. Rev. B: Condens. Matter **45**, 7959 (1992).
22. V. I. Belinicher, A. L. Chernyshev, and V. A. Shubin, Phys. Rev. B: Condens. Matter **53**, 335 (1996).
23. N. M. Plakida and V. S. Oudovenko, Phys. Rev. B: Condens. Matter **59**, 11 949 (1999).
24. M. M. Korshunov, V. A. Gavrichkov, S. G. Ovchinnikov, I. A. Nekrasov, Z. V. Pchelkina, and V. I. Anisimov, Phys. Rev. B: Condens. Matter **72**, 165 104 (2005).
25. W. Stephan and P. Horsch, Phys. Rev. Lett. **66**, 2258 (1991).
26. R. Preuss, W. Hanke, and W. von der Linden, Phys. Rev. Lett. **75**, 1344 (1995).
27. V. F. Elesin and V. A. Kashurnikov, Zh. Éksp. Teor. Fiz. **106** (6), 1773 (1994) [JETP **79** (6), 961 (1994)].
28. B. I. Shraiman and E. D. Siggia, Phys. Rev. Lett. **61**, 467 (1988).
29. S. A. Trugman, Phys. Rev. Lett. **65**, 500 (1990).
30. A. F. Barabanov, R. O. Kuzian, L. A. Maksimov, and G. V. Uimin, Sverkhprovodimost: Fiz., Khim., Tekh. **3**, 8 (1990).
31. A. F. Barabanov, R. O. Kuzian, and L. A. Maksimov, J. Phys.: Condens. Matter. **39**, 129 (1991).
32. A. P. Kampf, Phys. Rev. **249**, 219 (1994).
33. G. Dorf, A. Muramatsu, and W. Hanke, Phys. Rev. B: Condens. Matter **41**, 9264 (1990).
34. S. Sahrakorpi, R. S. Markiewicz, H. Lin, M. Lindroos, X. J. Zhou, T. Yoshida, W. L. Yang, T. Kakeshita, H. Eisaki, S. Uchida, S. Komiya, Y. Ando, F. Zhou, Z. X. Zhao, T. Sasagawa, A. Fujimori, Z. Hussain, Z.-X. Shen, and A. Bansil, Phys. Rev. B: Condens. Matter **78**, 104 513 (2008).
35. T. R. Thurston, R. J. Birgeneau, M. A. Kastner, N. W. Preyer, G. Shirane, Y. Fujii, K. Yamada, Y. Endoh, K. Kakurai, M. Matsuda, Y. Hidaka, and T. Murakami, Phys. Rev. B: Condens. Matter **40**, 4585 (1989).
36. S. M. Hayden, G. Aeppli, H. Mook, D. Rytz, M. F. Hundley, and Z. Fisk, Phys. Rev. Lett. **66**, 821 (1991).
37. D. Mihailovic and V. V. Kabanov, Struct. Bonding **114**, 331 (2005).
38. I. M. Lifshitz, Zh. Éksp. Teor. Fiz. **38**, 1569 (1960) [Sov. Phys. JETP **11**, 1130 (1960)].
39. I. M. Lifshitz, M. Ya. Azbel, and M. I. Kaganov, *Electron Theory of Metals* (Nauka, Moscow, 1971; Consultants Bureau, New York, 1973).
40. J. W. Loram, J. Luo, J. R. Cooper, W. Y. Liang, and J. L. Tallon, Phys. Chem. Solids **62**, 59 (2001).
41. Ya. B. Gaididei and V. M. Loktev, Phys. Status Solidi B **147**, 307 (1988).
42. V. A. Gavrichkov, S. G. Ovchinnikov, A. A. Borisov, and E. G. Goryachev, Zh. Éksp. Teor. Fiz. **118** (2), 422 (2000) [JETP **91** (2), 369 (2000)].
43. J. Zaanen, G. A. Sawatzky, and J. W. Allen, Phys. Rev. Lett. **55**, 418 (1985).
44. V. V. Val'kov and S. G. Ovchinnikov, *Quasiparticles in Strongly Correlated Systems* (Siberian Branch of the Russian Academy of Sciences, Novosibirsk, 2001) [in Russian].
45. R. O. Zaĭtsev, Zh. Éksp. Teor. Fiz. **68** (1), 207 (1975) [Sov. Phys. JETP **41** (1), 100 (1975)].
46. M. M. Korshunov and S. G. Ovchinnikov, Eur. Phys. J. B **57**, 271 (2007).
47. N. M. Plakida and V. S. Oudovenko, Zh. Éksp. Teor. Fiz. **131** (2), 259 (2007) [JETP **104** (2), 230 (2007)].
48. V. V. Val'kov and D. M. Dzebisashvili, Zh. Éksp. Teor. Fiz. **127** (3), 686 (2005) [JETP **100** (3), 608 (2005)].
49. H. Shimahara and S. Takada, J. Phys. Soc. Jpn. **60**, 2394 (1991); J. Phys. Soc. Jpn. **61**, 989 (1992).
50. A. F. Barabanov and V. M. Berezovskiĭ, Zh. Éksp. Teor. Fiz. **106** (4), 1156 (1994) [JETP **79** (4), 627 (1994)].
51. A. Sherman and M. Schreiber, Phys. Rev. B: Condens. Matter **65**, 134 520 (2002).
52. A. A. Vladimirov, D. Ile, and N. M. Plakida, Teor. Mat. Fiz. **145** (2), 240 (2005) [Theor. Math. Phys. **145** (2), 1576 (2005)].
53. A. F. Barabanov, A. A. Kovalev, O. V. Urazaev, A. M. Belemuk, and R. Hayn, Zh. Éksp. Teor. Fiz. **119** (4), 777 (2001) [JETP **92** (4), 677 (2001)].
54. S. Sachdev, A. V. Chubukov, and A. Sokol, Phys. Rev. B **51**, 14874 (1995).
55. A. V. Chubukov and D. K. Morr, Phys. Rep. **288**, 355 (1997).
56. L. Hozoi, M. S. Laad, and P. Fulde, Phys. Rev. B: Condens. Matter **78**, 165 107 (2008).
57. M. Hashimoto, T. Yoshida, H. Yagi, M. Takizawa, A. Fujimori, M. Kubota, K. Ono, K. Tanaka, D. H. Lu, Z.-X. Shen, S. Ono, and Y. Ando, Phys. Rev. B: Condens. Matter **77**, 094 516 (2008).
58. M. Platé, J. D. F. Mottershead, I. S. Elfimov, D. C. Peets, Ruixing Liang, D. A. Bonn, W. N. Hardy, S. Chiuzbaian, M. Falub, M. Shi, L. Patthey, and A. Damascelli, Phys. Rev. Lett. **95**, 077001 (2005).
59. A. Ino, C. Kim, M. Nakamura, T. Yoshida, T. Mizokawa, A. Fujimori, Z.-X. Shen, T. Kakeshita, H. Eisaki, and S. Uchida, Phys. Rev. B: Condens. Matter **65**, 094504 (2002).
60. M. M. Korshunov and S. G. Ovchinnikov, Fiz. Tverd. Tela (St. Petersburg) **45** (8), 1351 (2003) [Phys. Solid State **45** (8), 1415 (2003)].
61. U. Tutsch, P. Schweiss, H. Wühe, B. Obst, and Th. Wolf, Eur. Phys. J. B **41**, 471 (2004).

62. F. Onufrieva and P. Pfeuty, Phys. Rev. B: Condens. Matter **61**, 799 (2000).

63. I. Tsukada and S. Ono, Phys. Rev. B: Condens. Matter **74**, 134 508 (2006).

64. D. Le Boeuf, N. Doiron-Leyraud, J. Levallois, R. Daon, J.-B. Bonnemaison, N. E. Hussey, L. Balicas, B. J. Ramshaw, R. Liang, D. A. Bonn, W. N. Hardy, S. Adachi, C. Proust, and L. Taillefer, Nature **450**, 533 (2003).

65. T. Adachi, T. Noji, and Y. Koike, Phys. Rev. B: Condens. Matter **64**, 144 524 (2001).

66. N. P. Ong, Phys. Rev. B: Condens. Matter **43**, 193 (1991).

67. R. Daon, N. Doiron-Leyraud, D. LeBoeuf, S. Y. Li, F. Laliberté, O. Cyr-Choiniére, Y. J. Jo, L. Balicas, J.-Q. Yan, J.-S. Zhou, J. B. Goodenough, and L. Taillefer, Nat. Phys. **5**, 31 (2009).

68. A. Kaminski, S. Rosenkranz, N. M. Fretweel, M. R. Norman, M. Randeria, J. C. Campuzano, J.-M. Park, Z. Z. Li, and H. Raffy, Phys. Rev. B: Condens. Matter **73**, 174 511 (2006).

69. A. A. Kordyuk, S. V. Borisenko, M. Khupfer, and J. Fink, Phys. Rev. B: Condens. Matter **67**, 064504 (2003).

70. J. G. Storey, J. L. Tallon, and G. V. M. Williams, Phys. Rev. B: Condens. Matter **78**, 140506(R) (2008).

71. S. Hufner, M. A. Hossain, A. Damascelly, and G. A. Sawatzky, Rep. Prog. Phys. **71**, 062501 (2008).

Translated by N. Wadhwa